Experimental and Numerical Study on Drag Reduction Performance of Slickwater in Turbulent Pipeflow

Fan Fan, Fujian Zhou[(✉)], and Zhiyu Liu

Unconventional Gas Institute of China University of Petroleum, Beijing, China
zhoufj@cup.edu.cn

Abstract. This paper aims to build a simplified friction prediction modeling of polymer drag reduction in pipeflows on the basis of the Giesekus constitutive equation, which was validated by the loop experiment and field application. The model is used to calculate the drag reduction of polyacrylamide tetrapolymer additive (i.e., DR800) in a turbulent pipeflow. Based on the stress balance equation, a double integration is applied to get the friction coefficient of DR800. Although the physical mechanism has still not been clearly identified, the modeling is introduced to explain the contribution of different components: Reynolds shear stress, viscous shear stress, and viscoelastic shear stress. Extensive experimental measurements of the DR effect were performed at different Reynolds numbers to valid the modeling. By consistent comparisons between modeling with experimental results and field application, an insight into DR mechanism of slickwater is obtained. With the numerical simulation and a laboratory experiment, the drag reduction performance of DR800 can be predicted in a range, which expects to provide some guidance and reference for field operation.

Keywords: Drag reduction · Slickwater · Turbulent · Pipeflow · Polymer

1   Introduction

In recent years, due to the increased number of ultra-deep wells and extended scale of SRV fracturing in tight reservoirs, drag reduction performance of slickwater is more and more valued and has become an important factor of fracturing, especially for unconventional tight reservoirs, where hydraulic fracturing and horizontal drilling play essential roles [1]. It is generally known that slickwater has an overwhelming advantage on creating more fractures or complex fracture network thus maximizing the initial production rate, which has been constantly indicated by field experience. However, hydraulic fracturing requires a high pumping rate thus to dramatically increases operation friction, so slickwater is used to reduce friction loss [2].

Slickwater, whose main component is long-chain polymer (such as polyacrylamide, polyethylene oxide, guar, and guar derivatives), is a water-based low-viscosity fracturing fluid [3]. The fact that polymer/surfactant added at low concentration to wall-bounded turbulent flows leads to a dramatic friction reduction has been known for several decades [4]. Since DR phenomenon was discovered, a bulk of applications was discovered, such as reducing energy consumption, increasing flow rate, and decreasing pump displacement in turbulent pipeflow systems [5]. However, even as the most promising agent, it is difficult to accurately simulate and forecast the drag reduction rate of drag reducer (DR%). In the past 40 years, extended experimental and numerical works from various fields have been conducted to understand how the polymer behaves. However, because DR% is affected by the polymer concentration, temperature, salinity, and the roughness of the tube, the exact mechanism for the drag reduction is still poorly understood [3–7]. And a lot of mathematical models were set up to describe the drag reducer behavior from the distribution pattern of drag reducer, which can mainly be separated into three categories: the influence of drag reducer on the change of macroscopic fluid flow state, which is represented by boundary layer theory; drag reducer changes the turbulent structure to reduce the flow energy consumption, which is represented by the turbulence suppression theory; flexible structure of drag reducer changes when flows, which is represented by the viscoelastic drag reduction theory [6]. But those mathematical models are performed under a premise that DRA is time-averaged and has uniform spatial distribution. And few researches consider the dynamic microstructure changes in the flow process. In the following research, the changes of the dynamic microstructure are considered.

In this paper, a simplified modeling is put forward to calculate the drag reduction of polyacrylamide tetrapolymer additive (i.e., DR800) in a turbulent pipeflow. Based on the stress balance equation, a model is introduced to explain the contribution of different shear stress: viscous shear stress, Reynolds shear stress, and viscoelastic shear stress. The modeling also tries to explain how the friction reduction rate changes with the concentration of DR800, which has much to do with the conformation tensor of the polymer solution. Thus to verify this modeling, a laboratory friction loop test was set up for accurately characterizing the friction reduction property under different concentrations, the results of which show consistency with the modeling. In particular, a visualization window is set for observing the dynamic microstructure changes in the flow process. By consistent comparisons between modeling with experimental results and field application, an insight into DR mechanism of slickwater is obtained.

And some parameters related to temperature in models are expected to improve to fit the oil field better.

2 Numerical Process

As is shown in Fig. 1, a pipeflow is introduced as the calculation area under cylindrical coordinate system.
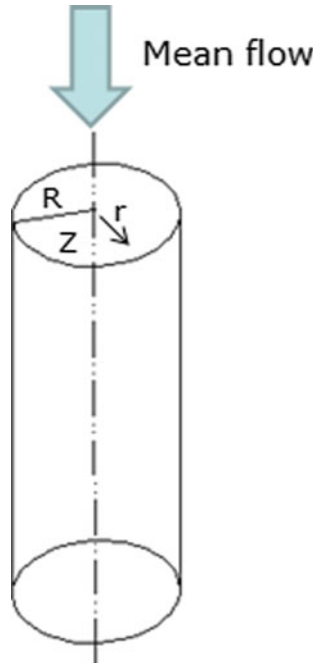

Fig. 1. Pipeflow geometry model

Firstly, measure the apparent shear viscosities and extensional viscosities of the polymer solution by HAKKE rheometer. Then qualitatively describe the measured shear viscosities and extensional viscosities using Giesekus model [7]. By applying the Giesekus model, the governing equations for dynamic motion of the polymer solution are:

Continuity equation:

$$\frac{\partial u}{\partial z} = 0 \tag{1}$$

Momentum equation:

$$\frac{\partial u_i}{\partial t} + u_j \frac{\partial u_i}{\partial z_j} = -\frac{1}{\rho}\frac{\partial p}{\partial z_j} + \frac{\mu}{\rho}\frac{\partial}{\partial z_j}\left(\frac{\partial u_i}{\partial z_j}\right) + \frac{1}{\lambda\rho}\frac{\partial c_{ij}}{\partial z_j} \tag{2}$$

Giesekus Constitutive equation:

$$\tau_{ij} + \lambda\left(\frac{\partial \tau_{ij}}{\partial t} + \frac{\partial u_m \tau_{ij}}{\partial z_m} - \frac{\partial u_i}{\partial z_m}\tau_{mj} - \frac{\partial u_j}{\partial z_m}\tau_{im} + \frac{\alpha}{\eta}\tau_{im}\tau_{mj}\right)$$
$$= \eta\left(\frac{\partial u_i}{\partial z_j} + \frac{\partial u_j}{\partial z_i}\right) \tag{3}$$

where λ and α are the relaxation time and the mobility factor, respectively; η is a ratio of additive contributions to the zero-shear rate solution viscosity; μ are dynamic viscosity. Take pipe radius R as characteristic length, friction speed U_τ as characteristic speed thus to introduce non-dimensional variables as follows:

$$r^* = \frac{r}{R}, \quad t^* = \frac{t}{R/U_\tau}, \quad u^* = \frac{u_i}{U_\tau}, \quad p^* = \frac{p - P}{\rho U_\tau^2}, \quad z^* = \frac{z}{l} \tag{4}$$

The Bulk Reynolds is defined as:

$$\mathrm{Re_b} = \frac{2U_\mathrm{b}R}{v} \tag{5}$$

Local skin friction coefficient $C_{\mathrm{f}(x,t)}$ is defined as:

$$C_\mathrm{f}(x, t) = \frac{2\tau}{\rho U_\mathrm{b}^2} = \frac{8}{\mathrm{Re_b}}\frac{\mathrm{d}u}{\mathrm{d}z}\Big|_{z=0} \tag{6}$$

The Reynolds-averaged Navier–Stokes equation in the z-direction for an impressible pipeflow is given on the basis of several defined dimensionless quantities and averaging operators:

$$-\frac{\partial p^*}{\partial z^*} = \frac{1}{r^*}\frac{\partial}{\partial r}r^*\left[\overline{u_r u_z} - \frac{1}{\mathrm{Re_b}}\frac{\partial u_z^*}{\partial r^*}\right] + \frac{\partial u_z^*}{\partial t^*} + \beta\frac{C_{rz}}{We_\tau} \tag{7}$$

where

$$\beta = \frac{\eta}{\mu} \tag{8}$$

Then a direct relationship between C_f and Reynolds stress distribution is obtained by applying a double integration $\int_{-1}^{1} r^* \int_{-1}^{r^*} r^* \mathrm{d}r^* \mathrm{d}r^*$:

$$C_\mathrm{f} = \frac{16}{\mathrm{Re_b}} + 4\int_0^1 2r^*\overline{u_r^* u_z^*} \cdot r^*\mathrm{d}r^* + 4\int_0^1 2r^*\beta\frac{C_{rz}}{We_r} \cdot r^*\mathrm{d}r^* \tag{9}$$

The equation can show the contribution of different components, this method, named as the FIK integration, was first proposed by Fukagata et al. to evaluate active turbulent

control in 2002. It is extended for friction prediction of slickwater in this paper. The first term of the friction factor is viscous contribution, which is identical to the Newton fluid. The second term, turbulence contribution, is proportional to the weighted average of the Reynolds shear stress [8]. The weightings indicate that Reynolds stress has different contributions to turbulence at different locations. The smaller the distance to the wall is, the greater the contribution of Reynolds stress to turbulence. The third term, viscoelastic contribution, describes the difference between Newtonian fluid and the polymer additive fluid, in which C_{rz} (conformation tensor) characterizes the internal state of polymer solution. And from physics perspective, we can think of it as a physical quantity that describes the degree of molecular deformation. And from previous study, construction tensor can be calculated by [9].

$$C_{rz} = \langle \underline{R_r}\,\underline{R_z} \rangle = \frac{1}{R_o^2} \int R_r R_z \Psi(r,z,t)\mathrm{d}r \qquad (10)$$

where R_r, R_z is used to represent the macromolecular chain end vector, R_0^2 is the mean square radius of rotation of the macromolecule, and particularly for DR800 (whose main content is diacrylamide dimethyl propane sulfonic acid) $R_0^2 = 0.23 \times 10^{-7}$ m. $\Psi(r,z,t)$ is the macromolecular configuration spatial distribution function, which varies with location in the axis and flow time.

However, it is really difficult to know the exactly distribution function under each velocity and concentration. So calculation can be simplified in the following way. From previous study [10] into C_{rz}, the second-order macromolecule orientation tensor $\langle \underline{R_r}\,\underline{R_z} \rangle$, is symmetric, which has three orthogonal feature vector a_1, a_2, a_3. The feature values represent the quantity of macromolecular along the corresponding direction. Take 0.07% polymer addictive as an example, the polymer in the solution has uniform distribution as shown in Fig. 2 the polymer molecules are evenly distributed in three major axes, so $a_1 = a_2 = a_3 = \begin{pmatrix} 1/3 & 0 & 0 \\ 0 & 1/3 & 0 \\ 0 & 0 & 1/3 \end{pmatrix}$. And $a_1 = a_2 = a_3 = \begin{pmatrix} 1 & 0 & 0 \\ 0 & 1 & 0 \\ 0 & 0 & 1 \end{pmatrix}$ for 0.01% polymer addictive as shown in Fig. 3. $a_1 = a_2 = a_3 = \begin{pmatrix} 1/2 & 0 & 0 \\ 0 & 1/2 & 0 \\ 0 & 0 & 1/2 \end{pmatrix}$. for 0.03% polymer addictive as shown in Fig. 4. In that way, C_{rz} under different concentration (namely 0.01, 0.03, 0.07, 0.10 wt%) can be approximately calculated. But for other concentrations, macromolecular microstructure has no apparent feature.

Dispersed pipeflow geometry model mentioned in Fig. 1 to 1,126,320 O-type grids by Fluent, as shown in Fig. 5.
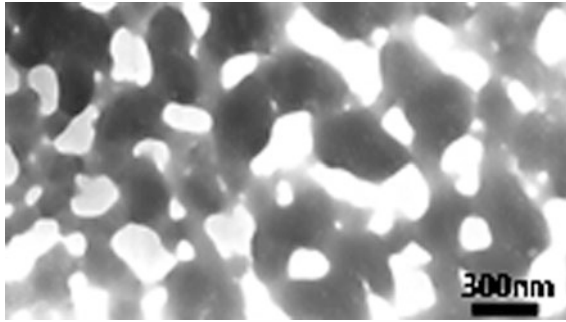
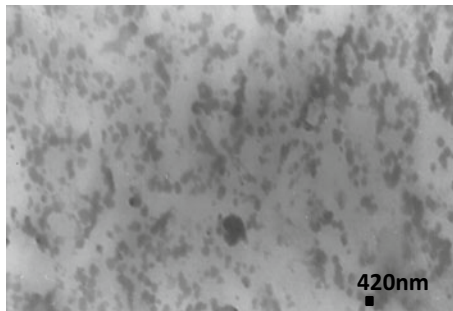**Fig. 2.** TEM image of 0.07 wt% polymer addictive

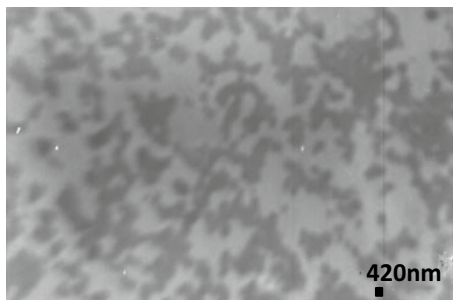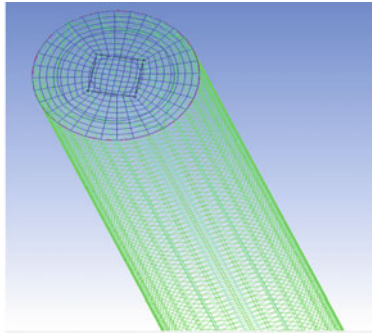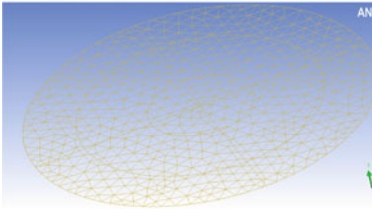**Fig. 3.** TEM image of 0.01 wt% polymer addictive

Fig. 4. TEM image of 0.03 wt% polymer addictive

(a) Side view of the geometry model

(b) Top view of the geometry model

Fig. 5. Mesh generation

To avoid meaningless oscillating pressure field, make a staggered mesh with P* in center and velocity component around the corner. Adams–Bashforth format is adapted to discrete the control equation. DR% is defined as DR $= \frac{C_{fo} - C_f}{C_{fo}} \times 100\%$, where C_{fo} is the fanning friction coefficient of water, and C_f is the friction coefficient of the slickwater under the same displacement. Then the following results can be obtained as shown in Figs. 6, 7, 8, 9 and 10.
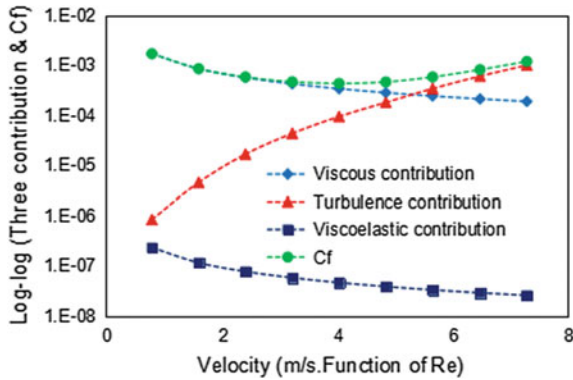

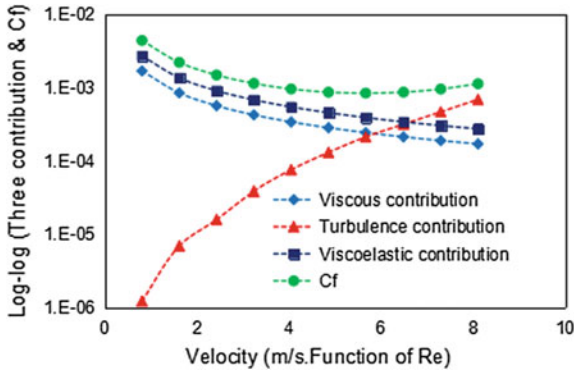**Fig. 6.** Contribution at different velocity (0.01 wt%DR800)

Fig. 7. Contribution at different velocity (0.03 wt%DR800)
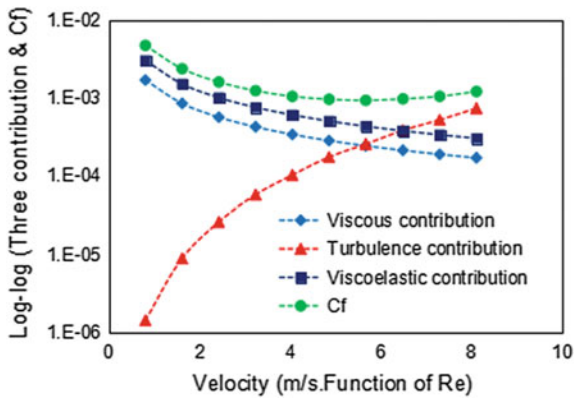

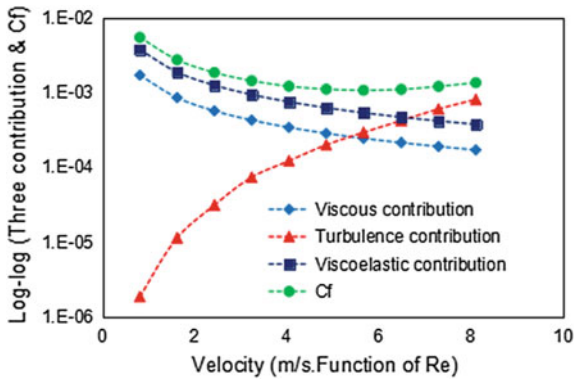**Fig. 8.** Contribution at different velocity (0.07 wt%DR800)

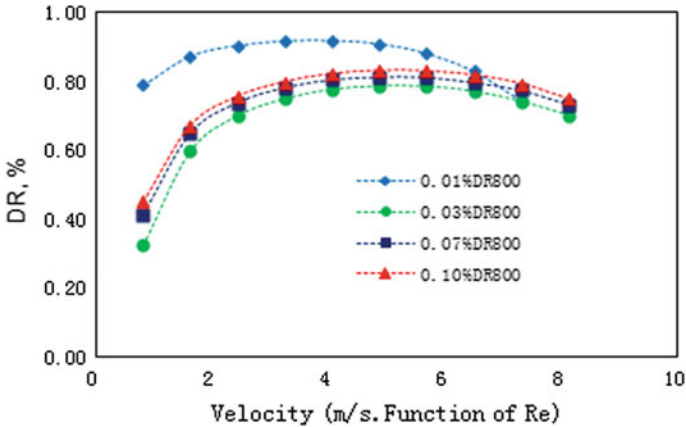**Fig. 9.** Contribution at different velocity (0.10 wt%DR800)

**Fig. 10.** DR% of different concentration of DR800

From the calculation of the three contribution items, some observations can be listed as follows: (1) As the complexity of the flow increases, the viscous contribution and viscoelastic contribution decreases, whereas the turbulence contribution increases; (2) In low Reynolds numbers, viscoelastic shear stress contributes most to friction coefficient while the turbulence can be neglected; (3) In high Reynolds numbers, the contribution of turbulence increases rapidly thus to be the dominating part of the overall contribution, followed by viscoelasticity and the least is viscous shear stress; (4) Under large velocity, macromolecular chain may suffer shear damage from pump; therefore, DR becomes smaller.

3   Experimental Process

3.1   Equipment Composition

A schematic diagram of the experimental apparatus is shown in Fig. 11. It was a closed-loop system consisted of a pumping system, pipeline testing system, pressure sensing systems, data acquisition system, and other measurement instruments. The pumping system includes ① water tank (50 L), ② effluent tank (70 L), ③ solution tank (50 L), ④ a screw pump, whose maximum pumping rate is 2.5 m³/h. To better simulate flow conditions in the field, solution tank is equipped with a heater for changing fluid temperature, ⑤ flow stabilizer, a 10 L intermediate accumulator with airbag inflated with nitrogen, which can absorb the pulse energy of the fluid from the pump, thus to reduce the turbulence of flow.

The pipeline testing system mainly consists of five parts: ① absolute pressure transducer, ② three 3-m-long straight pipelines with different inside diameters (6 mm, 8 mm, and 10 mm) and ball valves on both ends and a differential pressure transducer (0–0.5 MPa, ±0.02%), to minimize the additional shear effect from the corners connected to each tube, pressure taps were located 0.25 m away from both ends to measure
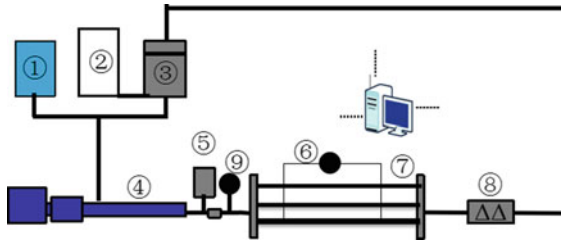
(a) Schematic diagramt

(b) Real object picture

Fig. 11. Schematic diagram and real object picture of friction loop testing platform

the 2.5 m-pressure drop, ③ temperature sensor (0–100 °C, ±0.1 °C), ④ mass flowmeter (0–3 m^3/h, ±0.001 m^3/h), used for monitoring flow in the loop and providing feedback to the screw pump for fine tuning, ⑤ visual tube window (10 cm long), for better observing whether drag reducer agent distributes evenly. And the corresponding real object picture is shown as in Fig. 11b.

3.2   Equipment Reliability

Before experiments, the reliability of equipment needs to be checked. For circular tube, the pressure drop of water across the three tubes was tested, respectively, and compared with the results calculated by the Prandtl–Karman correlation [Eq. (11)], which is typically used to describe the turbulent behavior of Newtonian fluids in smooth tubes [11], so it can be the judgment basis of experimental accuracy and reliability for pipeline section.

$$\frac{1}{\sqrt{C_f}} = 2\lg\left(\mathrm{Re}\sqrt{C_f}\right) - 0.8 \tag{11}$$

And as shown in Fig. 12, the experimental data points are well distributed over the rate set base near the quasi-line, which indicating the experiment device has high accuracy and are able to provide strong evidence for the drag reduction experiment reliability.
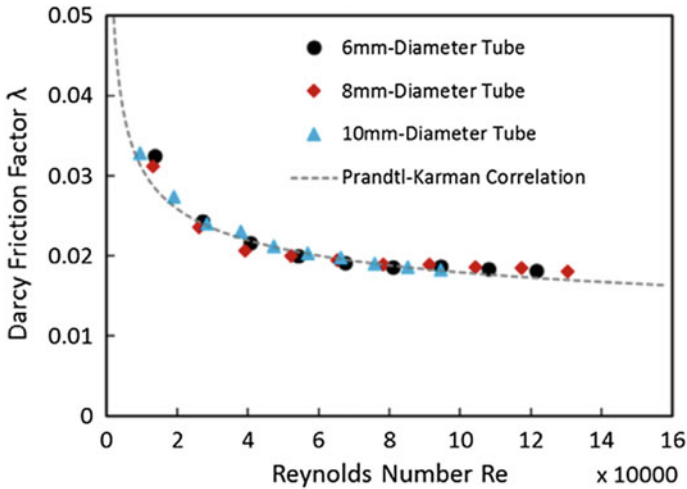
Fig. 12. Comparison of experimental measurement with calculation results
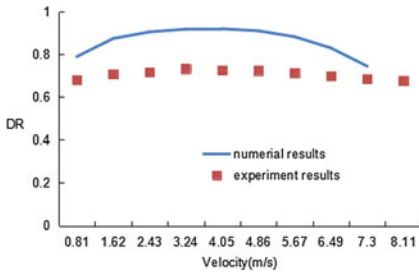
4 Results Comparison of Numerical with Laboratory Test

Based on the indoor friction loop testing platform, hundreds of experiments for measuring friction coefficient were carried out, and to make the results comparison convincing, error was minimized by averaging C_f from lots of repeated experiments under each velocity. And as shown in Fig. 13, the prediction results agreed well with experimental results, which indicate the discussion based on numerical analysis is supportive. And the method for simplifying C_{rz} combining macromolecular microstructure in polymer solution is feasible.
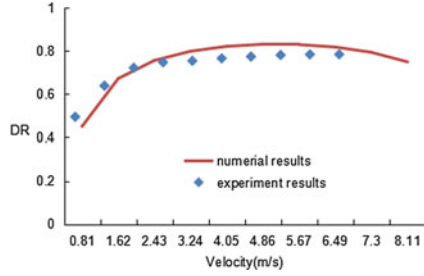
Based on the results comparison of numerical with indoor test under different concentration, we can see that the modeling is not well-fitting for low concentration. And in high velocity, numerical results show a downward trend, which may be a result of neglecting the influence of temperature on reducing viscosity.

5 Field Application

In order to further verify the indoor model and serve the field better, on-site friction tests of related wells were carried out. Well 18 was chosen for friction reduction test, which is located in Zhaojiawan Village, Gaolin Town, Yulin County, Shanxi Province. The well structure used for the test was the upper 15,876 mm oil pipes, its length recorded as 1525 m; the lower 12,662 mm oil pipes, its length recorded as 1212 m. The concentration of polymer for on-site test is 0.08%. Then the measured results can be obtained with pressure meters placed in wellhead and well bottom as shown in Table 1.
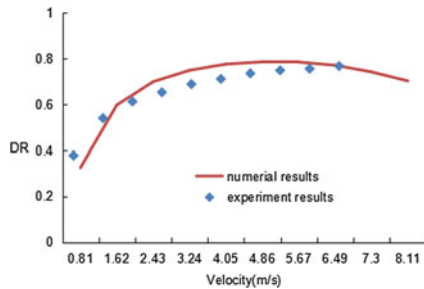
(a) Results comparison under 0.01wt%DR800

(b) Results comparison under 0.03wt%DR800
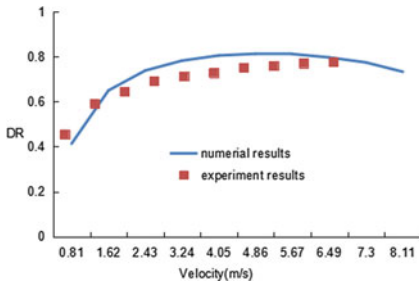
(c) Results comparison under 0.07wt%DR800

(d) Results comparison under 0.10wt%DR800

Fig. 13. Results comparison of numerical with indoor test under different concentration

Table 1 On-site measured results of slickwater

No.	Pumping rate (m^3/min)	Measured DR%
1	0.6	74.14
2	0.9	78.37
3	1.2	80.24
4	1.5	81.30
5	1.8	81.99
6	2.1	82.47
7	2.4	82.83
8	2.7	83.11
9	3.0	83.33

Comparison between measured results and model predictions of slickwater can be concluded by transforming displacement (m^3/min) to velocity (m/s), as shown in Fig. 14, the drag reduction performance of DR800 can be predicted in a range. While for more precise prediction in high velocity, some factors in models are expected to be considered to fit the field better, such as the positive influence of temperature on reducing viscosity thus to increase DR, which needs continuous effort from all.
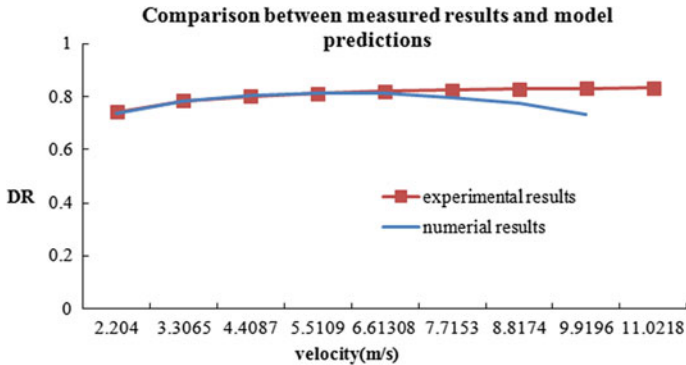
Fig. 14. Comparison between measured results and model predictions

6   Conclusions

Numerical stimulation and experiments were performed for the fully developed turbulence flow of polymer solution under different concentration in pipeflow in this paper. With the numerical simulation and a laboratory experiment, the drag reduction performance of DR800 can be predicted in a range, which provides some guidance and reference for field operation. The conclusions are as follows: (1) As the complexity of the flow increases, the viscous contribution and viscoelastic contribution decreases, while the turbulence contribution increases. (2) In low Reynolds numbers, viscoelastic shear stress contributes most to friction coefficient while the turbulence can be neglected. (3) In high Reynolds numbers, the contribution of turbulence increases rapidly thus to be the dominating part of the overall contribution, followed by viscoelasticity and the least is viscous shear stress. (4) Under large velocity, macromolecular chain may suffer shear damage from pump; therefore, DR becomes smaller. (5) In high velocity, numerical results show a downward trend, which is inconsistent with the fact, it may be a result of neglecting the influence of temperature on reducing viscosity of slickwater.

References

1. EIA. Initial production rates in tight oil formations continue to rise. Today in energy. U.S. Energy Information Administration (EIA). [WWW Document]. 2016.
2. Moosaie A. DNS of turbulent drag reduction in a pressure-driven rod-roughened channel flow by microfiber additives. J Nonnewton Fluid Mech. 2016;232:1–10.
3. Liang T, Yang Z, Zhou F, et al. A new approach to predict field-scale performance of friction reducer based on laboratory measurements. J Petrol Sci Eng. 2017;159:927–33.
4. Yu B, Li F, Kawaguchi Y. Numerical and experimental investigation of turbulent characteristics in a drag-reducing flow with surfactant additives. Int J Heat Fluid Flow. 2004;25(6):961–74.
5. Fukagata K, Iwamoto K, Kasagi N. Contribution of Reynolds stress distribution to the skin friction in wall-bounded flows. Phys Fluids. 2002;14(11):L73–6.

6. Carreau PJ, Grmela M. Conformation tensor rheological models. J Nonnewton Fluid Mech. 1987;23(23):271–94.
7. Yang Z. Study on drag reduction characteristics and models of Slickwater fracturing fluid. Beijing: China University of Petroleum. 2017.
8. Liu D, Wang Q, Wei J. Experimental study on drag reduction performance of mixed polymer and surfactant solutions. Chem Eng Res Des. 2018.
9. Sitaramaiah G, Smith CL. Turbulent drag reduction by polyacrylamide and other polymers. Soc Petrol Eng J. 1969;9(2):183–8.
10. Li Y-H, Chesnut GR, Richmond RD, Beer GL, Caldarera VP. Laboratory tests and field implementation of gas-drag-reduction chemicals. SPE Prod Facil. 1998;13:53–8.
11. Shah SN. Effects of pipe roughness on friction pressures of fracturing fluids. SPE Prod Eng. 1990;5:151–6.